Prepatterning by RhoGEFs governs Rho GTPase spatiotemporal dynamics during wound repair

Mitsutoshi Nakamura, Jeffrey M. Verboon, and Susan M. Parkhurst

Basic Sciences Division, Fred Hutchinson Cancer Research Center, Seattle, WA

Like tissues, single cells are subjected to continual stresses and damage. As such, cells have a robust wound repair mechanism comprised of dynamic membrane resealing and cortical cytoskeletal remodeling. One group of proteins, the Rho family of small guanosine triphosphatases (GTPases), is critical for this actin and myosin cytoskeletal response in which they form distinct dynamic spatial and temporal patterns/arrays surrounding the wound. A key mechanistic question, then, is how these GTPase arrays are formed. Here, we show that in the *Drosophila melanogaster* cell wound repair model Rho GTPase arrays form in response to prepatterning by Rho guanine nucleotide exchange factors (RhoGEFs), a family of proteins involved in the activation of small GTPases. Furthermore, we show that Annexin B9, a member of a class of proteins associated with the membrane resealing, is involved in an early, Rho family–independent, actin stabilization that is integral to the formation of one RhoGEF array. Thus, Annexin proteins may link membrane resealing to cytoskeletal remodeling processes in single cell wound repair.

Introduction

Cells undergo continuous stress, both mechanical and chemical, which can lead to ruptures in the cell membrane and damage to the underlying cortex (McNeil and Steinhardt, 1997; Sonnemann and Bement, 2011; Cooper and McNeil, 2015). Cells with noncatastrophic damage can undergo single cell repair and remain functional. As such, cells in a variety of organisms and tissues have been shown to have a robust cellular wound repair response that is composed of rapid membrane resealing and dynamic cytoskeletal repair at the cell cortex, presumably in response to an influx of calcium (Bement et al., 1999; McNeil and Kirchhausen, 2005; Abreu-Blanco et al., 2011a). However, the extent to which these distinct aspects of single cell wound repair are molecularly and physically coupled remains unclear.

Early single cell wound repair studies proposed a mechanism for membrane resealing termed the membrane patch hypothesis (McNeil et al., 2000). This hypothesis involves the rapid recruitment of intracellular vesicles upon wounding, followed by their fusion to each other and the surrounding membrane to form a temporary plug, and has been confirmed by live imaging studies in *Xenopus laevis* (Terasaki et al., 1997; Cooper and McNeil, 2015; Davenport et al., 2016).

Equally important to membrane repair is cytoskeletal repair at the cell cortex. This process is mediated by actin and myosin II accumulating at the wound edge to form an actomyosin ring that then translocates inward, resulting in wound closure (Fig. 1 A; Bement et al., 1999; Mandato and Bement, 2003; Abreu-Blanco et al., 2011a,b; Sonnemann and Bement, 2011). One group of proteins that is indispensable for this cytoskeletal response during cell wound repair is the Rho family of GTPases. Rho GTPases cycle between GTP- and GDP-bound forms, which is mediated by Rho guanine nucleotide exchange factors (RhoGEFs), Rho GTPase activating proteins (RhoGAPs), and Rho guanine nucleotide dissociation inhibitors (RhoGDIs; Fritz and Pertz, 2016; Hodge and Ridley, 2016). GTP-bound Rho family GTPases regulate actin and myosin dynamics through interacting effector proteins (Jaffe and Hall, 2005). During many processes, spatiotemporal patterning of Rho family GTPases is an important aspect of actin and myosin regulation. Studies in *Xenopus* and *Drosophila melanogaster* have shown that the Rho GTPase family proteins Rho, Rac, and Cdc42 are localized in specific patterns (arrays) with significant temporal and spatial overlap surrounding the wound (Fig. 1, A–D″; and Video 1; Benink and Bement, 2005; Vaughan et al., 2011; Burkel et al., 2012; Abreu-Blanco et al., 2014; Verboon and Parkhurst, 2015). Relatively little is known to date about how these arrays are formed and if/how their formation is linked to the initial calcium signal and membrane patch.

Results and discussion

RhoGEFs, RhoGAPs, and RhoGDIs are strong candidates to be the molecules needed to set up and/or maintain the distinct Rho family GTPase patterns/arrays formed in response to cell

Correspondence to Susan M. Parkhurst: susanp@fredhutch.org

Abbreviations used: Anx, Annexin; ChFP, mCherry fluorescent protein; eGFP, enhanced GFP; GEF, guanine nucleotide exchange factor; LatB, latrunculin B; NC, nuclear cycle; Pbl, pebble; RhoGAP, Rho GTPase activating protein; RhoGDI, Rho guanine nucleotide dissociation inhibitor; sfGFP, super folder GFP.

The Rockefeller University Press
J. Cell Biol. Vol. 216 No. 12 3959–3969
https://doi.org/10.1083/jcb.201704145

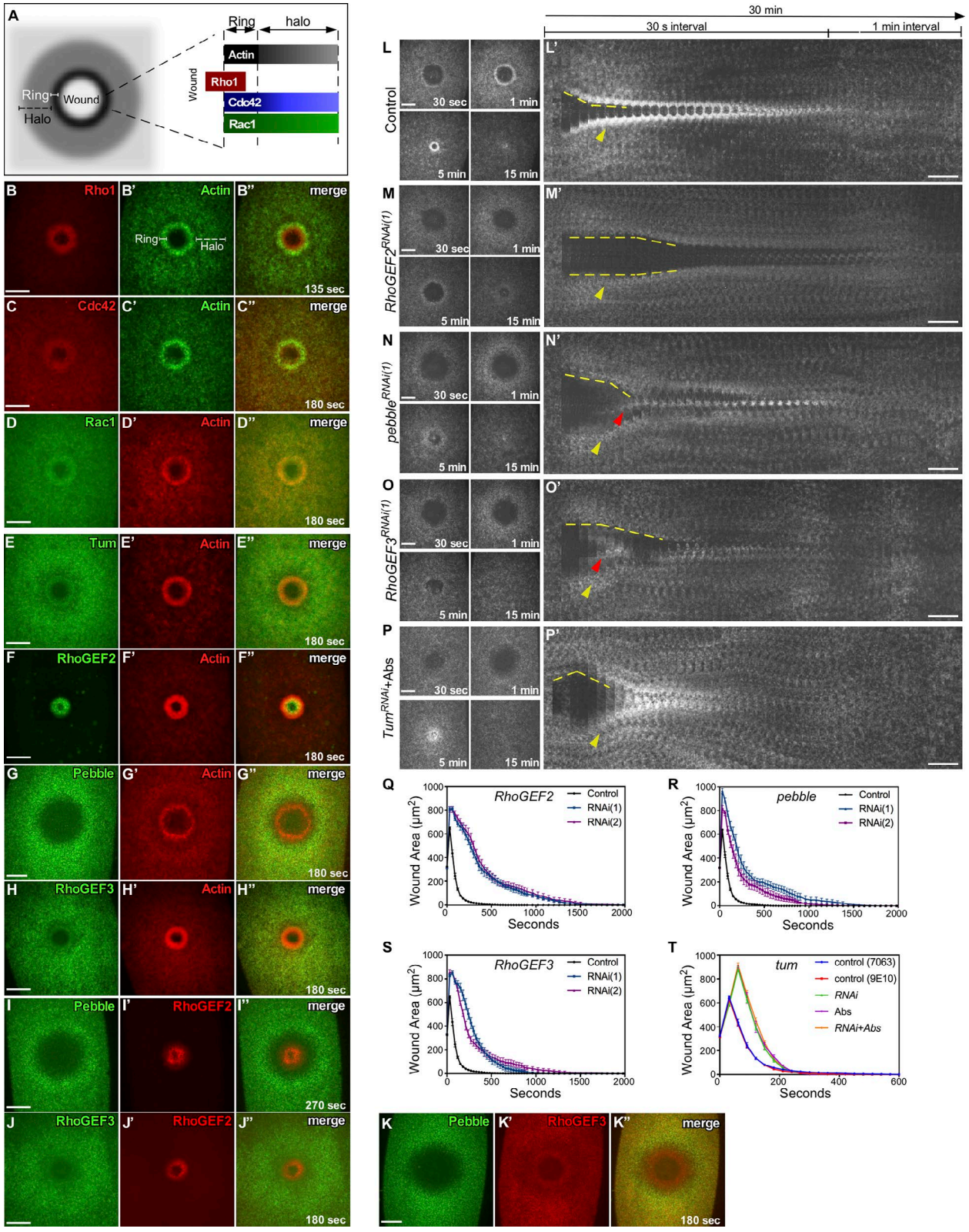

Figure 1. **RhoGEF2, Pbl, RhoGEF3, and Tum exhibit discrete localization patterns and are required for cell wound repair.** (A) Schematic diagram summarizing the localization patterns of actin, Rho1, Rac1, and Cdc42 at cell wounds. (B–H) Confocal xy projection images from *Drosophila* NC4–6 staged embryos coexpressing an actin marker (sGMCA or sChMCA) and fluorescently tagged Rho family GTPases: ChFP-Rho1 (B–B″), ChFP-Cdc42 (C–C″), and GFP-Rac1 (D–D″). The actin ring and halo regions are indicated in (B′). (E–H) Confocal xy projection images from *Drosophila* NC4–6 staged embryos coexpressing sChMCA and GFP-tagged RhoGEFs or Tum: sfGFP-Tum (E–E″), sfGFP-RhoGEF2 (F–F″), Pbl-eGFP (G–G″), and sfGFP-RhoGEF3 (H–H″). (I–K) Confocal xy projection images from *Drosophila* NC4–6 staged embryos coexpressing two fluorescently tagged RhoGEFs: Pbl-eGFP and RFP-RhoGEF2 (I–I″), sfGFP-RhoGEF3 and RFP-RhoGEF2 (J–J″), and Pbl-eGFP and sfGFP-RhoGEF3 (K–K″). (L–P) Actin dynamics (sChMCA or sGMCA) during cell wound repair in control (GAL4 driver 7063 alone) (L), *RhoGEF2*$^{RNAi(1)}$ (M), *pbl*$^{RNAi(1)}$ (N), *RhoGEF3*$^{RNAi(1)}$ (O), and *Tum-i*+antibodies (Abs) (P). (L′–P′) xy Kymograph across

wounds. Hence, we wounded embryos containing one of the nine available GFP-tagged RhoGAP, 12 available GFP-tagged RhoGEF, or one GFP-tagged RhoGDI proteins combined with a fluorescent actin reporter (sChMCA [spaghetti squash driven, mCherry fluorescent protein {ChFP}, moesin-α-helical-coiled, and actin binding site]; see Materials and methods and Table S1; Kiehart et al., 2000; Wenzl et al., 2010; Abreu-Blanco et al., 2011a, 2014). Wounds were generated by laser ablation on the lateral side of nuclear cycle (NC) 4–6 *Drosophila* embryos (see Materials and methods). In control embryos, actin accumulates in two adjacent regions: (1) a highly enriched actin ring bordering the wound edge, and (2) an elevated actin halo encircling the actin ring (Fig. 1, A and B′). Of those examined, only one RhoGAP, tumbleweed (Tum), and three RhoGEFs, RhoGEF2, pebble (Pbl), and RhoGEF3, display a change in localization pattern and are recruited to areas surrounding the wound (Fig. 1, E–K″; Fig. S1; Fig. S2, A–A″ and H–K″; and Video 1). Tum, a RhoGAP, accumulates broadly at the wound, overlapping with the actin halo and ring, with an area of lower accumulation between the two (Fig. 1, E–E″; Fig. S2, A–A″ and L; and Video 1). RhoGEF2 localization is spatially restricted: it forms a ring-like array inside of and partially overlapping with the actin ring (Fig. 1, F–F″; Fig. S2, H–H″ and M; and Video 1). Pbl accumulates in a diffuse ring-like array overlapping with the actin halo region. Pbl overexpression (one or two copies of Pbl–enhanced GFP [eGFP]) slightly affects actin halo formation; however, the actin ring forms normally and the wounds close with normal kinetics (Fig. 1, G–G″; Fig. S2, I–J and N; and Video 1). RhoGEF3 accumulates in a broad but diffuse array in the actin halo region that partially overlaps with the actin ring (Fig. 1, H–H″; Fig. S2, K–K″ and O; and Video 1). We also examined the recruitment of RhoGEFs relative to each other in cell wounds. RhoGEF2 does not overlap with Pbl or RhoGEF3 (Fig. 1, I–J″; Fig. S2, P–R; and Video 1). However, although there is a clear gap between RhoGEF2 and Pbl localization arrays at the wound edge, RhoGEF2 and RhoGEF3 localization regions are adjacent. Pbl and RhoGEF3 localization arrays overlap in the actin halo region (Fig. 1, K–K″; Fig. S2, Q; and Video 1). Thus, whereas Tum accumulates broadly around the wound, RhoGEF proteins form distinct spatial arrays surrounding the wound.

To investigate the function of Tum, RhoGEF2, Pbl, and RhoGEF3 in cell wound repair, we examined actin dynamics via a fluorescent actin reporter upon wounding in each RhoGEF and RhoGAP mutant background. Knockdown was achieved by expressing two independent RNAi constructs for each RhoGEF in the female germline using the GAL4-UAS system (see "Materials and methods"; Fig. S2 MM and Table S1). Knocking down any of the three RhoGEFs results in delayed actin accumulation around the wound edge, wound overexpansion, and delayed repair (Fig. 1, M–O and Q–S; Fig. S2, S–X; and Video 2) compared with control (GAL4 driver only) wounds (Fig. 1, L–L′ and Q–S; Fig. S2, W and X; and Video 2). In addition, from 2 min after wounding, actin accumulates within the wound in $pbl^{RNAi(1)}$ and $RhoGEF3^{RNAi(1)}$ embryos (Fig. 1, N′ and O′). To knockdown Tum, we tested the one RNAi line available, and to confirm the phenotype, we injected monoclonal Tum antibodies into both control and tum^{RNAi} embryos. Tum knockdown results in only minor effects on the repair process: wound overexpansion and slightly delayed wound closure that is compensated for by slightly increased rates of expansion and closure (Fig. 1, P–P′ and T; Fig. S2, V–Y; and Video 2). Consistent with this, Rho1, Rac1, and Cdc42 are recruited to wounds in Tum antibody–injected embryos with only slightly changed patterns reflecting disruptions to actin (Fig. S2, B–G). Thus, RhoGEFs have a much stronger effect on cellular wound repair than Tum, and each RhoGEF displays a specific wound recruitment pattern reminiscent of the arrays formed by each of the Rho GTPases, supporting a model wherein RhoGEFs are involved in patterning the Rho GTPases, whereas the RhoGAPs work to refine rather than establish GTPase array patterns.

We next determined if the different RhoGEFs were acting upstream of a specific Rho family GTPase. We coexpressed each fluorescently tagged RhoGEF protein with each fluorescently tagged Rho GTPase (Fig. 2, A–R; and Video 3). The RhoGEF2 array formed at the wound overlaps with Rho1 completely and is mainly internal to, but slightly overlapping with, that of Rac1 and Cdc42 (Fig. 2, A–C″ and J–L; and Video 3). Pbl accumulation overlaps with that of Rac1 and Cdc42 in the halo region, but does not overlap with Rho1 (Fig. 2, D–F″and M–O; and Video 3). RhoGEF3 accumulation at wounds overlaps with Rac1 and Cdc42 in the halo and partially overlaps where they form a ring (Fig. 2, H–I″, Q, and R; and Video 3). RhoGEF3 overlap with Rho1 is minimal (Fig. 2, G–G″ and P; and Video 3). To further characterize their specificity, we examined the molecular interactions among the RhoGEFs and Rho family GTPases using GST pulldown assays. We find that RhoGEF2 and Pbl interact physically with GTP-bound Rho1 and, to a lesser extent, Cdc42-GTP, whereas RhoGEF3 interacts with Rac1-GTP (Fig. 2 S). Although these molecular interactions independently do not show one-to-one correspondence of RhoGEFs with Rho GTPases, they are consistent with RhoGEF2 regulating Rho1, whereas Pbl and RhoGEF3 regulate Cdc42 and/or Rac1.

We next examined changes to each GTPase array upon wounding in the different RhoGEF mutant backgrounds. *RhoGEF2*, *Pbl*, and *RhoGEF3* knockdown all led to varying degrees of actin disruption and wound repair defects, so we focused our analysis on the early events (array formation), comparing localization of the GTPase arrays in relation to the disrupted actin structures, and assessing wounds that were at a similar stage in the repair process instead of exactly matched time points (Fig. 3 and Video 4). In $RhoGEF2^{RNAi(1)}$ mutant embryos, Rho1 no longer accumulates in response to cell wounds (Fig. 3, B–B″and F; and Video 4), whereas Rac1 and Cdc42 still accumulate (Fig. 3, J–J″, N, R–R″, and V; and Video 4). Rac1 and Cdc42 predictably form arrays coincident with where the altered actin ring/halo is formed in these $RhoGEF2^{RNAi(1)}$ embryos. Consequently, we anticipated that Rac1 and Cdc42 array formation would be mislocalized or abrogated in relation to actin structures in $pbl^{RNAi(1)}$ and $RhoGEF3^{RNAi(1)}$ knockdown embryos. As expected, both Rac1 and Cdc42 showed mislo-

the wound area depicted in (L–P), respectively (yellow dashed lines, wound edges; yellow arrowheads, actin ring; red arrowheads, actin accumulation inside wounds). (Q–T) Quantification of the wound area over time for control, $RhoGEF2^{RNAi(1)}$, and $RhoGEF2^{RNAi(2)}$ (n = 10 for each; Q); control, $pbl^{RNAi(1)}$, and $pbl^{RNAi(2)}$ (n = 10 for each; R); control, $RhoGEF3^{RNAi(1)}$, and $RhoGEF3^{RNAi(2)}$ (n = 10 for each; S); and GAL4 control, 9E10 control, tum^{RNAi}, Tum Abs, and tum^{RNAi}+Abs (n = 10 for controls and n = 15 for tum^{RNAi} and Tum Abs; T). Time after wounding is indicated. Bars, 20 µm. Error bars represent ± SEM.

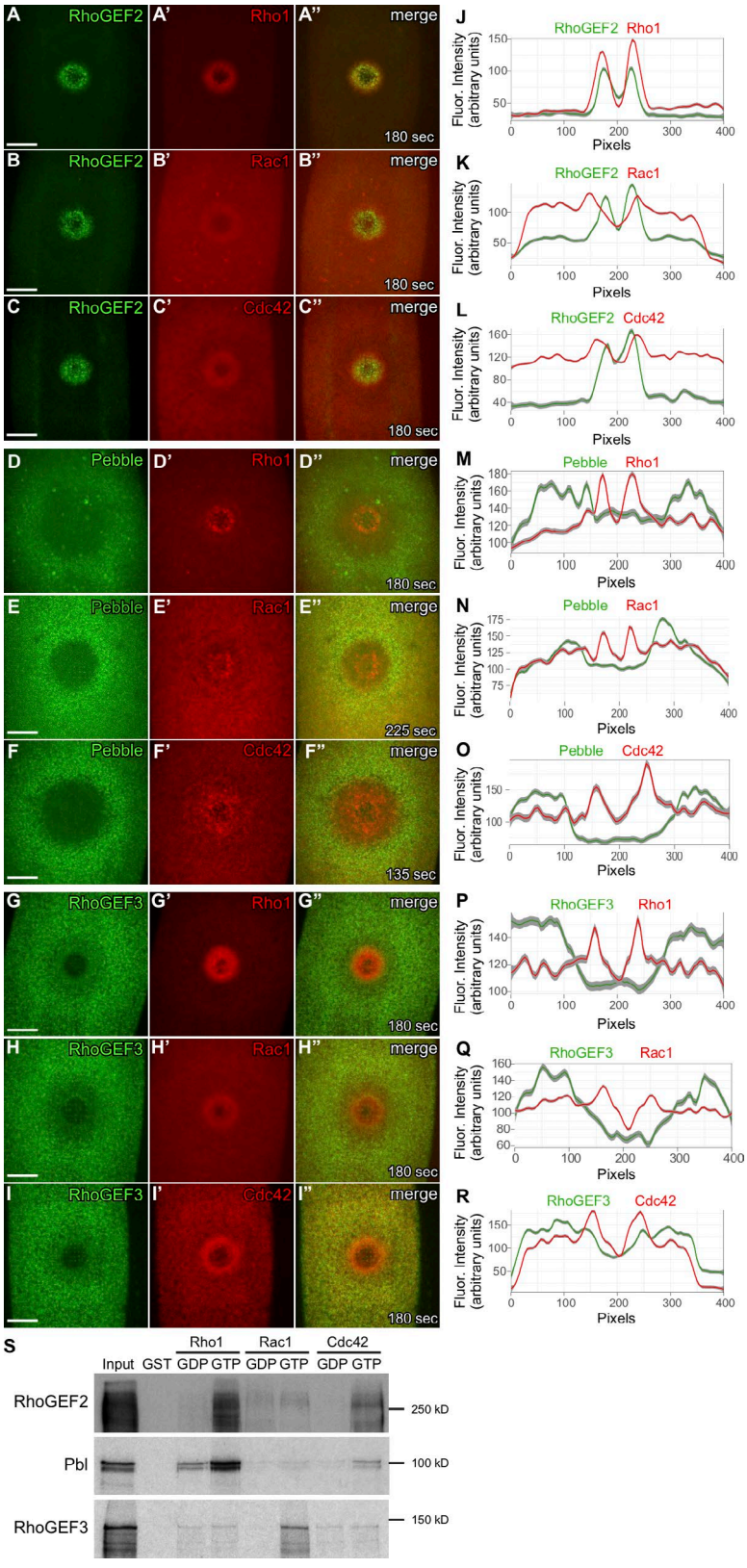

Figure 2. **RhoGEF2, Pbl, and RhoGEF3 interact with Rho1, Cdc42, and Rac1, respectively, during cell wound repair.** (A–I″) Confocal xy projection images at 180 s after wounding from *Drosophila* NC4–6 staged embryos coexpressing sfGFP-RhoGEF2 (A–C″), Pbl-eGFP (D–F″), or sfGFP-RhoGEF3 (G–I″) with ChFP-Rho1 (A–A″, D–D″, and G–G″), ChFP-Rac1 (B–B″, E–E″, and H–H″), or ChFP-Cdc42 (C–C″, F–F″, and I–I″). (J–R) Smoothened fluorescence (Fluor.) intensity (arbitrary units) profiles derived from averaged fluorescence intensity values over a 10-pixel width across the wound area in the embryo shown (A″–I″). Error bars represent the 95% confidence interval. (S) GST pulldown assays with ^{35}S-labeled in vitro translated RhoGEF2, Pbl, and RhoGEF3. The GST-Rho1, Rac1, and Cdc42 proteins were loaded with GDP or GTP as indicated. Time after wounding is indicated. Bars, 20 µm.

calized recruitment in these knockdown embryos: they exhibit complete, rather than partial, overlap with the Rho1 array at the wound interior, as well as accumulating at the wound edge and halo (Fig. 3, K–L″, O, P, S–T″, W, and X; and Video 4). In *pbl*$^{RNAi(1)}$ and *RhoGEF3*$^{RNAi(1)}$ knockdown embryos, Rho1 accumulates with the actin that is now found internal to the actin ring (Fig. 3, C–D″, G, and H; and Video 4). Thus, GEFs are clearly needed for the GTPase arrays to localize properly, suggesting that RhoGEFs are prepatterning the Rho GTPases. Taking together our colocalization results and their molecular

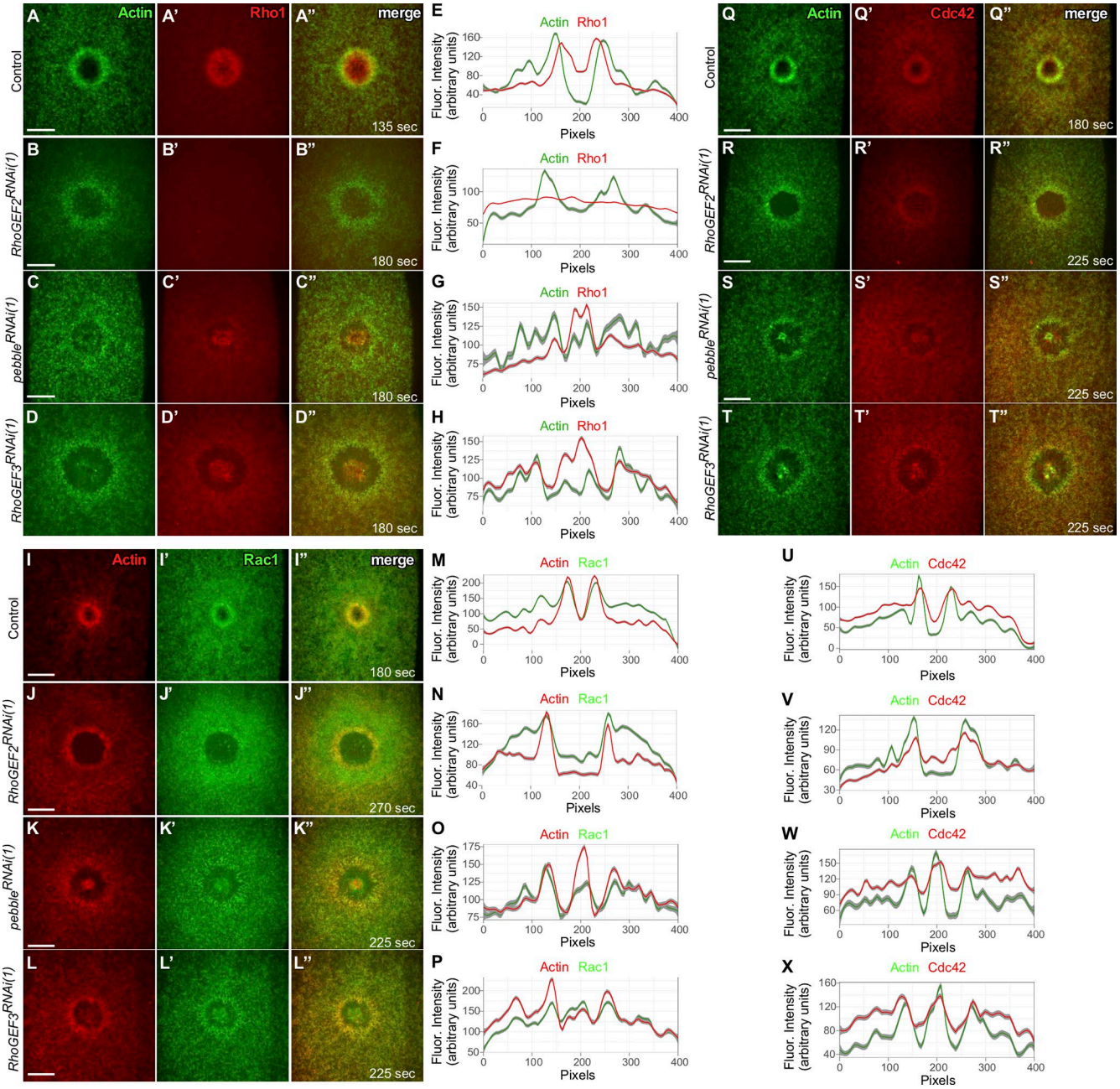

Figure 3. **Prepattern established by RhoGEFs is required for correct localization of Rho family GTPases.** (A–D) Localization of ChFP-Rho1 colabeled with sGMCA in control (A–A″), *RhoGEF2*$^{RNAi(1)}$ (B–B″), *pbl*$^{RNAi(1)}$ (C–C″), and *RhoGEF3*$^{RNAi(1)}$ (D–D″) mutant backgrounds. (E–H) Fluorescence intensity profiles across the wound area in (A″–D″). (I–L) Localization of GFP-Rac1 colabeled with sChMCA in control (I–I″), *RhoGEF2*$^{RNAi(1)}$ (J–J″), *pbl*$^{RNAi(1)}$ (K–K″), and *RhoGEF3*$^{RNAi(1)}$ (L–L″) mutant backgrounds. (M–P) Smoothened fluorescence (Fluor.) intensity (arbitrary units) profiles derived from averaged fluorescence intensity values over a 10-pixel width across the wound area in the embryo shown (I″–L″). Error bars represent the 95% confidence interval. (Q–T) Localization of ChFP-Cdc42 colabeled with sGMCA in control (Q–Q″), *RhoGEF2*$^{RNAi(1)}$ (R–R″), *pbl*$^{RNAi(1)}$ (S–S″), and *RhoGEF3*$^{RNAi(1)}$ (T–T″) mutant backgrounds. (U–X) Fluorescence intensity profiles across the wound area in (Q″–T″). Time after wounding is indicated. Bars, 20 µm.

(pulldown) specificities, we favor a model wherein RhoGEF3 and Pbl preferentially prepattern Rac1 and Cdc42, respectively. In contrast, RhoGEF2 not only specifically prepatterns Rho1 but also is indispensable for Rho1 accumulation at wounds. It is unclear why RhoGEF2-Rho1 shows more specificity than the other RhoGEF-Rho GTPase relationships, but it may be influenced by their acting in a more dynamic region of the wound that is largely interior to the cortical cytoskeleton.

To determine how RhoGEF arrays are themselves patterned, we examined the establishment of RhoGEF2 arrays in different RNAi- and drug-inhibited backgrounds. We focused on RhoGEF2 because of its specific spatial localization upon wounding and limited our analysis to the initial time points after wounding because, as repair progresses, GEF localization becomes increasingly influenced by cross talk among the RhoGEFs (Fig. S2, Z–FF″ and II–KK″; and Video 5). We first examined the accumulation of RhoGEF2 at wounds in which Rho1 or its downstream effectors were disrupted. Injection of embryos with C3 exoenzyme (Rho1 inhibitor) or Y-27632 (Rok inhibitor) had no effect on RhoGEF2 initial array formation, demonstrating

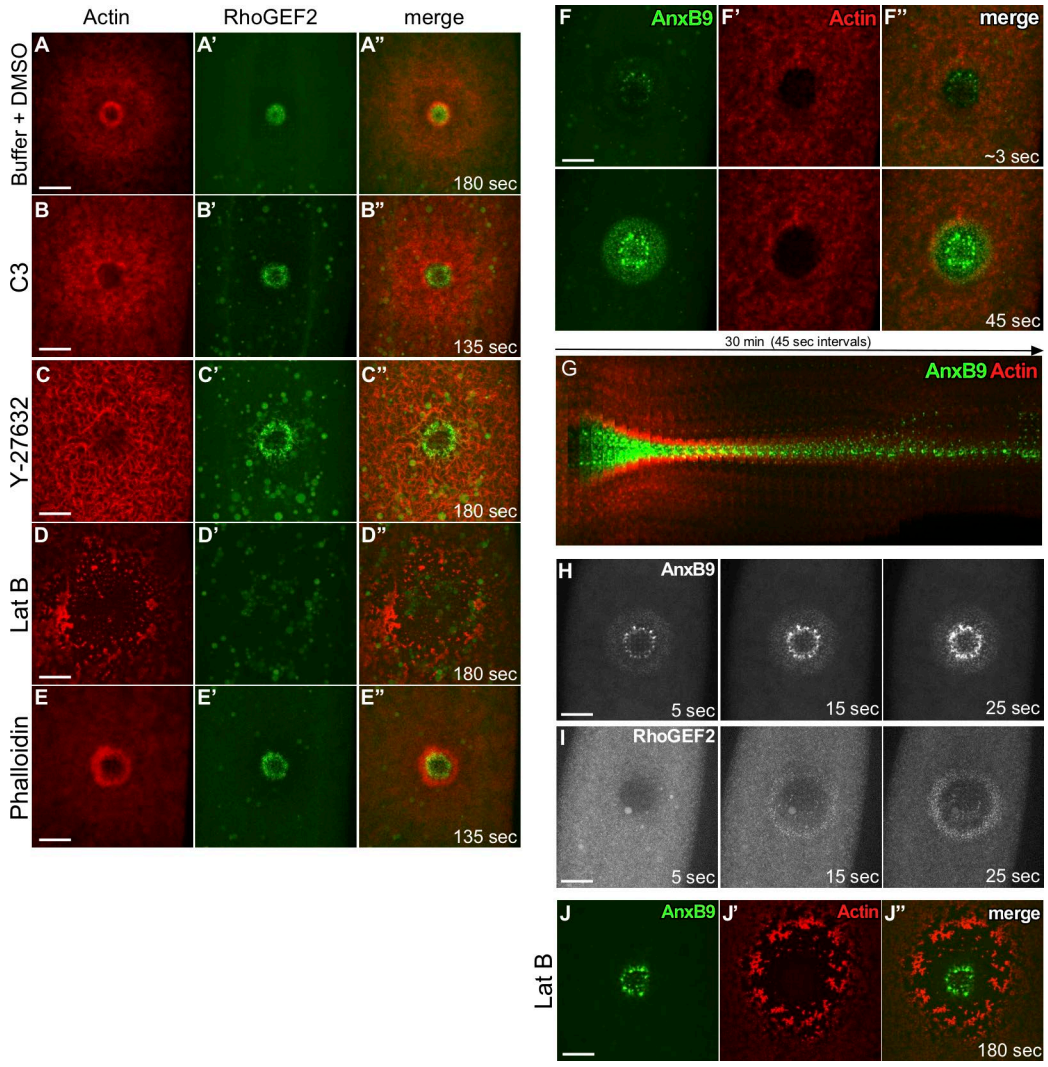

Figure 4. **RhoGEF2, but not AnxB9, accumulation at cell wounds is actin-dependent.** (A–E) Confocal xy projection images from *Drosophila* NC4–6 staged embryos coexpressing sfGFP-RhoGEF2 and sChMCA injected with injection buffer + 50% DMSO (control; A–A″), C3 exoenzyme (Rho1 inhibitor; B–B″), Y-27632 (Rok inhibitor; C–C″), LatB (depolymerizes F-actin; D–D″), and phalloidin (stabilizes F-actin; E–E″). (F–F″) Two confocal xy projection images at ∼3-s and 45-s time points from *Drosophila* NC4–6 staged embryos coexpressing eGFP-AnxB9 and sK2MCA. The fastest acquirable time point is labeled ∼3 s (G) xy Kymograph across the wound area from *Drosophila* NC4–6 staged embryos coexpressing eGFP-AnxB9 and sK2MCA. (H and I) Confocal xy projection images from *Drosophila* NC4–6 staged embryos expressing eGFP-AnxB9 (H) or sfGFP-RhoGEF2 (I) at three time points (5, 10, and 15 s). (J–J″) Confocal xy projection images from *Drosophila* NC4–6 staged embryos coexpressing eGFP-AnxB9 and sK2MCA that have been injected with LatB. Time after wounding is indicated. Bars, 20 µm.

that RhoGEF2 prepatterning is independent of feedback from Rho1 or its downstream effectors (Fig. 4, A–C″; and Video 5).

One molecule that did affect RhoGEF array formation throughout these studies was actin. RhoGEFs predictably followed altered actin structures, indicating that F-actin helps determine the formation and/or location of RhoGEF arrays. To test if disruption of F-actin affected RhoGEF2 localization at the wound, we disrupted normal actin function using latrunculin B (LatB) and phalloidin, which depolymerize or stabilize F-actin, respectively (Fig. 4, D–E″; and Video 5). Injection of LatB into embryos expressing super folder GFP (sfGFP)-RhoGEF2 and sChMCA results in depolymerization of the cortical actin cytoskeleton and the complete inability of the RhoGEF2 array to form at the wound (Fig. 4, D–D″; and Video 5). Injection of phalloidin into this background had no appreciable effect on wound repair dynamics other than actin accumulation remaining at the wound site after the wound was fully closed (Fig. 4, E–E″; and Video 5). Thus, stabilized F-actin allows for the accumulation of RhoGEF2 at the wound, is Rho family GTPases–independent, and is necessary for normal wound repair.

The striking necessity for stable F-actin for the initial RhoGEF2 array formation at wounds led us to examine cytoskeleton regulatory proteins that are involved early in wound repair. Annexins (Anxs), in particular, are of great interest because these proteins are fast-responding, are calcium-regulated, can form 2D lattices in vivo, and have been shown to accumulate at cell wounds (Blackwood and Ernst, 1990; Gerke et al., 2005; Bouter et al., 2015; Lauritzen et al., 2015). Anx proteins can also stabilize the cortical cytoskeleton, are involved in cell cortex remodeling during cytokinesis, and, interestingly, are membrane-binding proteins (Benaud et al., 2015; Gabel et al., 2015).

To test if Anx could mediate cytoskeletal changes required for RhoGEF2 array formation, we examined recruitment of GFP-AnxB9 upon wounding. AnxB9 accumulates incredibly

rapidly (<3 s) at the inside of the wound, overlapping slightly with the innermost edge of the actin ring (Fig. 4, F and G; Fig. S1, M, N, and YY; and Video 6). Importantly, AnxB9 accumulates at the wound before RhoGEF2, then settles into an accumulation that overlaps with RhoGEF2 (~45–60 s; Fig. 4, H and I). To determine if AnxB9 accumulation was upstream or downstream of early actin stabilization, we injected embryos expressing GFP-AnxB9 embryo with LatB and found that AnxB9 is still recruited to the wound in a similar spatiotemporal manner as in control embryos (Fig. 4 J and Video 6). These results indicate that AnxB9 could be the factor regulating the early actin stabilization necessary for RhoGEF2 array formation, because it accumulates at the wound with the right timing and localization and it occurs independently of actin stabilization.

Finally, to confirm that AnxB9 contributes to actin dynamics during cell wound repair, we wounded *AnxB9^{RNAi}* knockdown mutants. *AnxB9^{RNAi}* mutant embryos exhibit delayed actin accumulation around the wound edge, enhanced wound expansion, and delayed repair similar to *RhoGEF2^{RNAi}* mutants (Fig. 5, A–D; Fig. S2 MM; and Video 6). In addition, diffuse actin aberrantly accumulates within the wound (Fig. 5, B′–C′); however, the pattern is different from that observed in *pbl$^{RNAi(1)}$* and *RhoGEF3$^{RNAi(1)}$* embryos. To establish if RhoGEF2 was acting downstream of AnxB9, we examined RhoGEF2 localization patterns in the *AnxB9^{RNAi}* background. RhoGEF2 does not localize at the wound in *AnxB9^{RNAi}* mutant embryos (Fig. 5, E–E″; and Video 6). Interestingly, Pbl and RhoGEF3 still form arrays in this background, indicating specificity between AnxB9 and RhoGEF2 (Fig. S2, HH–HH″ and LL–LL″). Based on our results with LatB, we expected that AnxB9 is involved in a very early actin stabilization event that allows RhoGEF2 array formation. Thus, we stabilized actin by injecting phalloidin into *AnxB9^{RNAi}* mutant embryos. Strikingly, actin stabilization allows for partial rescue of RhoGEF2 recruitment to wounds: RhoGEF2 accumulates at the wound, albeit in an altered pattern, and the actin ring is less diffuse than in the *AnxB9^{RNAi}* background alone (Fig. 5, F–G″; and Video 6). Interestingly, the diffuse actin observed to accumulate at wound interiors in *AnxB9^{RNAi}* mutants may be the destabilized actin that AnxB9 normally stabilizes.

Spatiotemporal regulation of Rho GTPases is a critical aspect of their signaling activities. During *Drosophila* cell wound repair, we find that RhoGEF proteins prepattern the Rho family GTPases arrays necessary for cortical remodeling, whereas the Tum RhoGAP is involved in refining/sharpening these arrays (Fig. 5 H). Interestingly, we find that Rho1 array formation at cellular wounds consists of an AnxB9 → actin stabilization → RhoGEF2 → Rho1 pathway (Fig. 5 I). This pathway highlights an exciting requirement for actin stabilization early in the wound repair process, before Rho family GTPases arrive at the wound, and suggests that Anxs might be involved directly or indirectly in actin ring formation. Stabilizing actin may be important for RhoGEF recruitment and array formation by reinforcing the membrane plug attachment sites and/or forming a stable scaffold on which to assemble GEF arrays (Martin, 2010; Kapus and Janmey, 2013; Gefen and Weihs, 2016). Because Anx, RhoGEF, and Rho GTPase mutants delay but do not prevent wound closure, these proteins are required for increasing the speed of wound closure, whereas as yet unknown actin- and Rho-independent pathways may be required for closing the wounds. Future challenges include identifying the proteins needed for Pbl and RhoGEF3 array formation, as well as uncovering additional proteins involved in either membrane patching or cytoskeletal remodeling, which also impact this reciprocal process.

Materials and methods

Fly stocks and genetics

Flies are cultured and crossed at 25°C on yeast-cornmeal-molasses-malt medium. *Drosophila* has 26 RhoGEFs, 22 RhoGAPs, and 1 RhoGDI proteins. The flies used in this study are detailed in Table S1 (Kiehart et al., 2000; Buszczak et al., 2007; Wenzl et al., 2010; Abreu-Blanco et al., 2011a, 2014; Nagarkar-Jaiswal et al., 2015; Sarov et al., 2016). To drive expression in UAS flies, we used the P{w[+mC]=GAL4-nos.NGT}A driver. To knockdown genes, RNAi lines were driven maternally using the GAL4-UAS system by P{matalpha4-GAL-VP16}V37 (or P{matalpha4-GAL-VP16}V2H for driving *RhoGEF2$^{RNAi(1)}$* and *RhoGEF3$^{RNAi(1)}$* in the Pbl-eGFP background; Brand and Perrimon, 1993; Ni et al., 2011). All RNAi experiments were performed at least two times from individual genetic crosses.

Actin reporters

An actin reporter (sGMCA [spaghetti squash driven, GFP, moesin-α-helical-coiled and actin binding site]) was used to follow cortical cytoskeleton dynamics during wound repair (Kiehart et al., 2000). Equivalent actin reporters expressing mCherry (sChMCA; Abreu-Blanco et al., 2011a) or mKate2 (sK2MCA [spaghetti squash driven, mKate2 fluorescent protein, moesin-α-helical-coiled and actin binding site]) were also used. We generated sK2MCA by replacing the ChFP in sChMCA with mKate2 using standard molecular techniques.

Embryo handling and preparation

NC4–6 *Drosophila* embryos were collected from 0–30 min at room temperature (22°C). Embryos were hand dechorionated, dried for 5 min and placed onto No. 1.5 coverslips coated with strips of glue, then covered with Series 700 halocarbon oil (Halocarbon Products Corp.; Abreu-Blanco et al., 2011a).

GFP fusion protein screen for RhoGEFs, RhoGAPs, RhoGDI, and AnxB9 response to wounds

We examined ≥10 individual embryos from each RhoGEF, RhoGAP, RhoGDI, and AnxB9 listed in Table S1 to determine if their localization pattern changed upon wounding using time-lapse microscopy. Wound presence and size were confirmed using an actin reporter (sChMCA or sK2MCA). To quantify the wound response, we subtracted the GFP fluorescent intensity of the prewounding time point from the 180-s post-wounding image using Fiji software (Schindelin et al., 2012). We then measured the averaged GFP fluorescent intensity from 10 pixel sections across the wound in the subtracted image using Fiji (Fig. S1 A′″). Line profiles were plotted and the area under the curve was measured using Prism 7.0a (GraphPad Software Inc.). We set the threshold for nonresponse at 500 fluorescence units, which is not significantly different from our negative control (UAS-GFP expressed with maternal Gal4 driver; 159 fluorescence units), but significantly different from our positive control (the actin reporter sGMCA; 4780 fluorescence units).

Generation of transgenic flies

To generate spaghetti squash (sqh)-sfGFP-RhoGEF2, we modified the strategy previously described (Wenzl et al., 2010). UASp-RFP-RhoGEF2 was provided by J. Großhans, University of Göttingen, Göttingen, Germany (Wenzl et al., 2010). sfGFP was amplified and cloned into pBluescript as a 5′SwaI-3′HindIII. RhoGEF2 ORF was amplified from BDGP clone SD04476 and cut by SmaI (internal site), and two

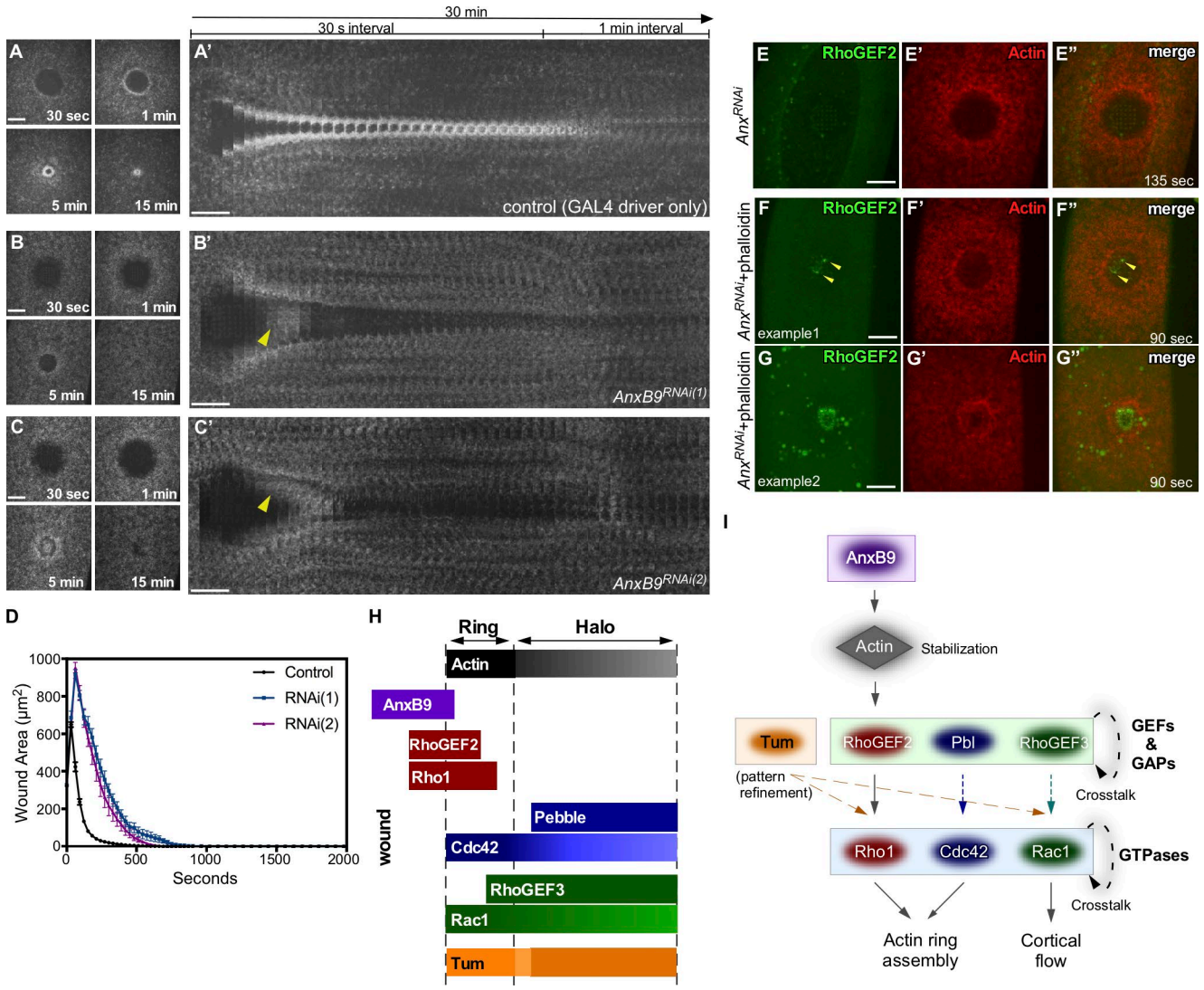

Figure 5. **Actin stabilization mediated by AnxB9 is required for RhoGEF2 recruitment to cell wounds.** (A–C) Actin dynamics during cell wound repair in control (GAL4 driver 7063 alone) (A), *AnxB9*$^{RNAi(1)}$ (B), and *AnxB9*$^{RNAi(2)}$ (C) NC4–6 staged embryos expressing an actin reporter (sGMCA). (A′–C′) xy Kymograph across the wound area in A–C, respectively. Arrowheads denote actin accumulation within the wound. (D) Quantification of the wound area over time (control, *AnxB9*$^{RNAi(1)}$, and *AnxB9*$^{RNAi(2)}$; $n = 10$ respectively). Error bars represent ± SEM (E–G″) Confocal xy projection images from *Drosophila* NC4–6 staged embryos coexpressing sfGFP-RhoGEF2 and sChMCA in an *AnxB9*^{RNAi} background injected with buffer (E–E″) or phalloidin (F–G″). RhoGEF2 partially accumulates at the wounds (arrowheads; F). (H) Schematic diagram summarizing the localization patterns of actin, AnxB9, RhoGEF2, Pbl, RhoGEF3, Tum, Rho1, Rac1, and Cdc42 at cell wounds. (I) Schematic diagram summarizing the pathways among AnxB9, actin, RhoGEFs, Tum, and Rho family GTPases in response to cell wounds. Time after wounding is indicated. Bars, 20 µm.

fragments were recovered by gel extraction. The N-terminal part of RhoGEF2 was cloned into pBluescript-sfGFP as a 5′HindIII-3′SmaI. Subsequently, the C-terminal part of RhoGEF2 was cloned into pBluescript-sfGFP-N-RhoGEF2 as a 5′SmaI-3′XbaI. sfGFP-RhoGEF2 was cut by SwaI and XbaI from pBluescript-sfGFP-RhoGEF2 and cloned into pSqh5′+3′UTR (Abreu-Blanco et al., 2011a) as a 5′StuI-3′XbaI fragment.

To generate sqh-Pbl-eGFP, Pbl-eGFP was amplified from UAS-Pbl-eGFP (provided by R. Saint, University of Melbourne, Victoria, Australia; Somers and Saint, 2003) fly genomic DNA and cloned into pSqh5′+3′UTR as a 5′StuI-3′XbaI fragment.

To generate UASp-sfGFP-RhoGEF3 and UASp-ChFP-RhoGEF3, the *RhoGEF3* ORF was amplified from BDGP clone LP23332 and fused 5′ to sfGFP or ChFP. Both sfGFP- and ChFP-RhoGEF3 fusions were cloned into pUASp as 5′KpnI-3′XbaI fragments.

To generate sqh-sfGFP-Tum, the *tum* ORF was amplified from genomic DNA prepared from UAS-Venus-Tum containing flies (provided by S. Gregory, University of Adelaide, North Terrace, Australia; Ebrahimi et al., 2010) and fused 5′ to sfGFP. The sfGFP-Tum fusion was cloned into pSqh5′+3′UTR (Abreu-Blanco et al., 2011a) as a 5′StuI-3′XbaI fragment.

RNAi lines for RhoGEF2$^{RNAi(2)}$ and RhoGEF3$^{RNAi(2)}$ were generated using the method previously described (Ni et al., 2011). Two oligos (shown here) were annealed and cloned into pWALIUM22: RhoGEF2$^{RNAi(2)}$, 5′-CTAGCAGTAACGGTTACTAGATTTATATATAGTTATATTCAAGCATATATATAAATCTAGTAACCGTTGCG-3′ and 5′-AATTCGCAACGGTTACTAGATTTATATATATGCTTGAATATAACTATATATAAATCTAGTAACCGTTACTG-3′; and RhoGEF3$^{RNAi(2)}$, 5′-CTAGCAGTCCGGGCGATTACTCAGACCAATAGTTATATTCAAGCATATTGGTCTGAGTAATCGCCCGGGCG-3′ and 5′-AATTCG

CCCGGGCGATTACTCAGACCAATATGCTTGAATATAACTATTG GTCTGAGTAATCGCCCGGACTG-3′.

To generate transgenic flies, each construct (500 µg/ml) was injected along with the pTURBO helper plasmid (100 µg/ml) into isogenic w^{1118} flies as previously described (Spradling, 1986). For generating RNAi transgenic lines, each construct (100 µg/ml) was injected into M{3xP3-RFP.attP}ZH-86Fb (24749) flies (Table S1). Transgenics were selected by eye color, and the insertions were mapped using standard genetic methods.

Other shRNAi lines used were generated by the DRSC/TRiP Functional Genomics Resources (Harvard Medical School) and obtained from the Bloomington Stock Center. Target sites of each RNAi line are as follows: RhoGEF2$^{RNAi(1)}$: 5′-TACGATGAGGTT CAAGAGATA-3′; RhoGEF3$^{RNAi(1)}$: 5′-CAACTCGATGTTACT GAACTA-3′; pbl$^{RNAi(1)}$: 5′-CTGAAGATTAATCAAACGAAA-3′; Anx$^{RNAi(1)}$: 5′-CCAGATCTTCCTCGAATACGA-3′; and Anx$^{RNAi(2)}$: 5′-CTGCAAGTCCAAGATCGACTA-3′.

Drug and antibody injections

Pharmacological inhibitors and antibodies were injected from the dorsal side into the center of NC4–6 staged *Drosophila* embryos, and laser wounding was performed 5 min after injection. The following inhibitors were used: C3 exoenzyme (1 mg/ml; Cytoskeleton, Inc., and Tocris Bioscience); Y-27632 (60 mM; Tocris Bioscience); LatB (0.5 mM; Millipore); and phalloidin (75 µg/ml; Thermo Fisher Scientific). C3 exoenzyme, Y-27632, and phalloidin were prepared in injection buffer (5 mM KCl and 0.1 mM NaP, pH 6.8). LatB was prepared in injection buffer + 10% DMSO. Injection buffer plus 50% DMSO was injected as a control. The following mouse mAbs were obtained from the Developmental Studies Hybridoma Bank: anti-c-myc (9E10), anti-Tum (1H5), and anti-Tum (2B6). All antibodies were dialyzed in PBS and concentrated before injection. The two Tum antibodies were mixed and injected into embryos at 120 ng/µl. A nonspecific antibody, 9E10, was injected into embryos as a control at 120 ng/µl.

Laser wounding

All wounds were generated with a pulsed nitrogen N2 Micropoint laser (Andor Technology Ltd.) tuned to 435 nm and focused on the cortical surface of the embryo. A region of interest was selected in the lateral midsection of the embryo, and ablation was controlled by Volocity (PerkinElmer) or MetaMorph (Molecular Devices). The mean ablation time was less than 3 s, and time-lapse imaging was initiated immediately. Occasionally, a faint grid pattern of fluorescent dots is visible at the center of wounds that arises from damaged vitelline membrane that covers embryos.

Live imaging

All imaging was performed in series 700 halocarbon oil at room temperature (22°C). Two microscopes were used. First, an Ultraview Vox spinning disk confocal system was used with a Yokogawa CSU-X1 confocal spinning disk head (PerkinElmer) mounted on a Nikon Eclipse Ti stand (Nikon Instruments) with a 60×/1.4 NA objective lens and controlled by Volocity software (v.5.3.0; PerkinElmer). Images and videos were acquired with 491 nm and 561 nm using a Hamamatsu C9100-13 EMCCD camera (PerkinElmer). Second, a Revolution WD Systems (Andor Technology Ltd.) mounted on a Leica DMi8 (Leica Microsystems Inc.) was used with a 63×/1.4 NA objective lens and controlled by MetaMorph software (Molecular Devices). Images and videos were acquired with 488 and 561 nm using an Andor iXon Ultra 897 EMCCD camera (Andor Technology Ltd.).

All images were 17–20-µm stacks/0.25-µm steps. For single color, images were acquired every 30 s for 15 min and then every 60 s for 25 min. For dual green and red colors, images were acquired every 45 s for 30–40 min.

Image processing, analysis, and quantification

Linear adjustments of brightness and contrast levels were applied using Fiji software (Schindelin et al., 2012). Wound areas were measured manually using Fiji. To generate xy kymographs, all time-lapse xy images were cropped to 5.8 × 94.9 µm, and then each cropped image was lined up using Fiji. To generate fluorescent profile plots, 10 pixel sections across the wound were generated using Fiji. The mean fluorescent intensity was calculated with R (Team, 2016) using the tiff package (Urbanek, 2013) to import the images. Line profiles were plotted with R using the ggplot2 package (Wickham, 2009) and fitted using the LOESS smoothing method with a span of 0.1 and using a line-plot to show the averaged fluorescence without smoothing. Line profiles from the left to right correspond to the top to bottom of the images unless otherwise noted.

Quantification of the wound expansion and closure rate was performed as follows: wound expansion was calculated with maximum wound area/initial wound size. Closure rate was calculated with two time points. One was t_{max} —that is, the time of reaching maximum wound area. The other was $t_{<half}$—that is, the time of reaching less than the half of maximum wound area using Microsoft Excel for Mac (2011). Using these time points, mean speed was calculated (wound area at t_{max} − wound area at $t_{<half}$/t_{max} − $t_{<half}$) with Microsoft Excel. Generation of all graphs and Student *t* tests were performed with Prism 7.0a (GraphPad Software Inc.). Figures were assembled in Canvas Draw 3 for Mac (Canvas GFX, Inc.).

GST pulldown assays

GST pulldown assays were performed as previously described (Abreu-Blanco et al., 2014). In brief, test proteins were synthesized in vitro using the TNT quick-coupled transcription-translation kit in the presence of ^{35}S-labeled methionine (Promega). For synthesizing RhoGEF2 and Tum proteins, each ORF was cloned into the pCite4 vector. RhoGEF3 and Pbl proteins were synthesized from BDGP clones LP23332 and SD01796, respectively (Drosophila Genomics Resource Center). The in vitro translated lysates were diluted in Hepes-LS buffer (20 mM Hepes, pH 7.5, 150 mM NaCl, 10% glycerol, 0.1% Triton X-100, and 1 mM DTT) with protease inhibitors (Complete EDTA-Free; Roche) and incubated in GST fused glutathione sepharose for 1 h at 4°C to remove nonspecific binding proteins. GST-Rho family GTPases were exchanged while bound to glutathione sepharose by incubating with either GDP or GMP-PNP in exchange buffer (50 mM Hepes, pH 7.08, 20 mM $MgCl_2$, 5 mM EDTA, 0.1 mM EGTA, 50 mM NaCl, and 0.1 mM DTT) for 30 min at 30°C. Exchange was performed immediately before use in pulldown assays. The precleared lysates were individually incubated with GST, GDP-bound Rho1, GTP-bound Rho1, GDP-bound Rac1, GTP-bound Rac1, GDP-bound Cdc42, or GTP-bound Cdc42 proteins in Hepes-LS for 1 h at 4°C. The beads were then washed 3 times in Hepes-LS buffer, and the bound fractions were analyzed by SDS-PAGE followed by autoradiography. In each case, 5% input is shown.

Quantification of mRNA levels in RNAi mutant backgrounds

Total RNA was obtained from 100 embryos (0–30 min old) using TRIzol (Invitrogen/Thermo Fisher Scientific) and then treated with DNase I (Sigma). Total RNA (1 µg) and oligo(dT) primers were used for reverse transcription with the ThermoScript RT-PCR System for First-Strand cDNA Synthesis (Invitrogen/Thermo Fisher Scientific) or the iScript Select cDNA Synthesis kit (Bio-Rad). RT-PCR analysis was performed using the validated primers (Hu et al., 2013) shown in the list below

and the iTaq Universal SYBR Green Supermix (Bio-Rad) with two individual parent sets and two technical replicates on the CFX96TM Real Time PCR Detection System (Bio-Rad). GAPDH1 was used as a reference gene. The percent knockdown was calculated using the ΔΔCq calculation method compared with control (GAL4 only). The following primers were used for this study: *GAPDH1*, 5′-TAAATTCGACTC GACTCACGGT-3′ and 5′-CTCCACCACATACTCGGCTC-3′; *tum*, 5′-AGTTATCAAGCGGGTGCCAA-3′ and 5′-ATGGTGCCTCCT TTGAAGGG-3′; *RhoGEF2*, 5′-TGAAAACGCAAGCAAATCTG-3′ and 5′-GATGCCACACCTTCTTCGAT-3′; *pbl*, 5′-ATCTGTTTG GCGACTATTTGGAT-3′ and 5′-GTTGCGAAAAACGCTTGCG-3′; *RhoGEF3*, 5′-GAGGAAACCAATCTGGTGGA-3′ and 5′-AGCCCT GTGCGCTATAAAGA-3′; and *AnxB9*, 5′-CAAGGCGATGAAAGG CTTCG-3′ and 5′-TGCCGTACGAGGTCTTGAAC-3′.

Online supplemental material

Fig. S1 shows the results from the GFP fusion protein screen for RhoGEFs, RhoGAPs, RhoGDI, and AnxB9 response to wounds. Fig. S2 shows the localization and mutant phenotypes of RhoGEF2, Pbl, RhoGEF3, and Tum during cell wound repair. Cross talk among RhoGEFs is needed to refine and/or maintain their arrays at cell wounds, but not to establish the initial GEF prepatterns. Table S1 describes all of the fly lines used in these studies. Video 1 shows the protein dynamics of Rho family GTPases, RhoGEFs, and Tum during cell wound repair. Video 2 shows the actin dynamics in controls and in Rho family GTPases, RhoGEFs, and Tum mutant backgrounds during cell wound repair. Video 3 shows a comparison of the localization among RhoGEFs and Rho family GTPases in response to cell wounds. Video 4 shows the dynamics of Rho family GTPases in RhoGEF mutant backgrounds. Video 5 shows RhoGEF2 localization in other RhoGEF mutant and drug injection backgrounds. Video 6 shows AnxB9 protein dynamics and mutant phenotypes in response to cell wounds.

Acknowledgments

We thank Maria Abreu-Blanco, Tony Cooke, Trish Gordon, Stephen Gregory, Jörg Groβhans, Kevin Jan, Jim Priess, Rob Saint, Johannes Sattmann, Scott Somers, the Bloomington and Kyoto Stock Centers, Vienna Drosophila Resource Center, Drosophila Genomics Resource Center, and the Harvard TRiP Project for advice, equipment, antibodies, flies, and other reagents used in this study.

This work was supported by National Institutes of Health grant GM111635 to S.M. Parkhurst.

The authors declare no competing financial interests.

Author contributions: All authors contributed to the design, execution, and interpretation of the experiments and to the writing of the manuscript.

Submitted: 24 April 2017
Revised: 17 August 2017
Accepted: 24 August 2017

References

Abreu-Blanco, M.T., J.M. Verboon, and S.M. Parkhurst. 2011a. Cell wound repair in *Drosophila* occurs through three distinct phases of membrane and cytoskeletal remodeling. *J. Cell Biol.* 193:455–464. http://dx.doi.org/10.1083/jcb.201011018

Abreu-Blanco, M.T., J.M. Verboon, and S.M. Parkhurst. 2011b. Single cell wound repair: Dealing with life's little traumas. *BioArchitecture.* 1:114–121. http://dx.doi.org/10.4161/bioa.1.3.17091

Abreu-Blanco, M.T., J.M. Verboon, and S.M. Parkhurst. 2014. Coordination of Rho family GTPase activities to orchestrate cytoskeleton responses during cell wound repair. *Curr. Biol.* 24:144–155. http://dx.doi.org/10.1016/j.cub.2013.11.048

Bement, W.M., C.A. Mandato, and M.N. Kirsch. 1999. Wound-induced assembly and closure of an actomyosin purse string in Xenopus oocytes. *Curr. Biol.* 9:579–587. http://dx.doi.org/10.1016/S0960-9822(99)80261-9

Benaud, C., G. Le Dez, S. Mironov, F. Galli, D. Reboutier, and C. Prigent. 2015. Annexin A2 is required for the early steps of cytokinesis. *EMBO Rep.* 16:481–489. http://dx.doi.org/10.15252/embr.201440015

Benink, H.A., and W.M. Bement. 2005. Concentric zones of active RhoA and Cdc42 around single cell wounds. *J. Cell Biol.* 168:429–439. http://dx.doi.org/10.1083/jcb.200411109

Blackwood, R.A., and J.D. Ernst. 1990. Characterization of Ca2(+)-dependent phospholipid binding, vesicle aggregation and membrane fusion by annexins. *Biochem. J.* 266:195–200. http://dx.doi.org/10.1042/bj2660195

Bouter, A., R. Carmeille, C. Gounou, F. Bouvet, S.A. Degrelle, D. Evain-Brion, and A.R. Brisson. 2015. Review: Annexin-A5 and cell membrane repair. *Placenta.* 36(Suppl 1):S43–S49. http://dx.doi.org/10.1016/j.placenta.2015.01.193

Brand, A.H., and N. Perrimon. 1993. Targeted gene expression as a means of altering cell fates and generating dominant phenotypes. *Development.* 118:401–415.

Burkel, B.M., H.A. Benink, E.M. Vaughan, G. von Dassow, and W.M. Bement. 2012. A Rho GTPase signal treadmill backs a contractile array. *Dev. Cell.* 23:384–396. http://dx.doi.org/10.1016/j.devcel.2012.05.025

Buszczak, M., S. Paterno, D. Lighthouse, J. Bachman, J. Planck, S. Owen, A.D. Skora, T.G. Nystul, B. Ohlstein, A. Allen, et al. 2007. The carnegie protein trap library: a versatile tool for Drosophila developmental studies. *Genetics.* 175:1505–1531. http://dx.doi.org/10.1534/genetics.106.065961

Cooper, S.T., and P.L. McNeil. 2015. Membrane Repair: Mechanisms and Pathophysiology. *Physiol. Rev.* 95:1205–1240. http://dx.doi.org/10.1152/physrev.00037.2014

Davenport, N.R., K.J. Sonnemann, K.W. Eliceiri, and W.M. Bement. 2016. Membrane dynamics during cellular wound repair. *Mol. Biol. Cell.* 27:2272–2285. http://dx.doi.org/10.1091/mbc.E16-04-0223

Ebrahimi, S., H. Fraval, M. Murray, R. Saint, and S.L. Gregory. 2010. Polo kinase interacts with RacGAP50C and is required to localize the cytokinesis initiation complex. *J. Biol. Chem.* 285:28667–28673. http://dx.doi.org/10.1074/jbc.M110.103887

Fritz, R.D., and O. Pertz. 2016. The dynamics of spatio-temporal Rho GTPase signaling: formation of signaling patterns. *F1000 Res.* 5:F1000 Faculty Rev-749. http://dx.doi.org/10.12688/f1000research.7370.1

Gabel, M., F. Delavoie, V. Demais, C. Royer, Y. Bailly, N. Vitale, M.F. Bader, and S. Chasserot-Golaz. 2015. Annexin A2-dependent actin bundling promotes secretory granule docking to the plasma membrane and exocytosis. *J. Cell Biol.* 210:785–800. http://dx.doi.org/10.1083/jcb.201412030

Gefen, A., and D. Weihs. 2016. Mechanical cytoprotection: A review of cytoskeleton-protection approaches for cells. *J. Biomech.* 49:1321–1329. http://dx.doi.org/10.1016/j.jbiomech.2015.10.030

Gerke, V., C.E. Creutz, and S.E. Moss. 2005. Annexins: linking Ca2+ signalling to membrane dynamics. *Nat. Rev. Mol. Cell Biol.* 6:449–461. http://dx.doi.org/10.1038/nrm1661

Hodge, R.G., and A.J. Ridley. 2016. Regulating Rho GTPases and their regulators. *Nat. Rev. Mol. Cell Biol.* 17:496–510. http://dx.doi.org/10.1038/nrm.2016.67

Hu, Y., R. Sopko, M. Foos, C. Kelley, I. Flockhart, N. Ammeux, X. Wang, L. Perkins, N. Perrimon, and S.E. Mohr. 2013. FlyPrimerBank: an online database for Drosophila melanogaster gene expression analysis and knockdown evaluation of RNAi reagents. *G3 (Bethesda).* 3:1607–1616. http://dx.doi.org/10.1534/g3.113.007021

Jaffe, A.B., and A. Hall. 2005. Rho GTPases: biochemistry and biology. *Annu. Rev. Cell Dev. Biol.* 21:247–269. http://dx.doi.org/10.1146/annurev.cellbio.21.020604.150721

Kapus, A., and P. Janmey. 2013. Plasma membrane--cortical cytoskeleton interactions: a cell biology approach with biophysical considerations. *Compr. Physiol.* 3:1231–1281.

Kiehart, D.P., C.G. Galbraith, K.A. Edwards, W.L. Rickoll, and R.A. Montague. 2000. Multiple forces contribute to cell sheet morphogenesis for dorsal closure in *Drosophila*. *J. Cell Biol.* 149:471–490. http://dx.doi.org/10.1083/jcb.149.2.471

Lauritzen, S.P., T.L. Boye, and J. Nylandsted. 2015. Annexins are instrumental for efficient plasma membrane repair in cancer cells. *Semin. Cell Dev. Biol.* 45:32–38. http://dx.doi.org/10.1016/j.semcdb.2015.10.028

Mandato, C.A., and W.M. Bement. 2003. Actomyosin transports microtubules and microtubules control actomyosin recruitment during Xenopus oocyte

wound healing. *Curr. Biol.* 13:1096–1105. http://dx.doi.org/10.1016/S0960-9822(03)00420-2

Martin, A.C. 2010. Pulsation and stabilization: contractile forces that underlie morphogenesis. *Dev. Biol.* 341:114–125. http://dx.doi.org/10.1016/j.ydbio.2009.10.031

McNeil, P.L., and T. Kirchhausen. 2005. An emergency response team for membrane repair. *Nat. Rev. Mol. Cell Biol.* 6:499–505. http://dx.doi.org/10.1038/nrm1665

McNeil, P.L., and R.A. Steinhardt. 1997. Loss, restoration, and maintenance of plasma membrane integrity. *J. Cell Biol.* 137:1–4. http://dx.doi.org/10.1083/jcb.137.1.1

McNeil, P.L., S.S. Vogel, K. Miyake, and M. Terasaki. 2000. Patching plasma membrane disruptions with cytoplasmic membrane. *J. Cell Sci.* 113:1891–1902.

Nagarkar-Jaiswal, S., P.-T. Lee, M.E. Campbell, K. Chen, S. Anguiano-Zarate, M.C. Gutierrez, T. Busby, W.-W. Lin, Y. He, K.L. Schulze, et al. 2015. A library of MiMICs allows tagging of genes and reversible, spatial and temporal knockdown of proteins in Drosophila. *eLife.* 4:e05338. http://dx.doi.org/10.7554/eLife.05338

Ni, J.-Q., R. Zhou, B. Czech, L.-P. Liu, L. Holderbaum, D. Yang-Zhou, H.-S. Shim, R. Tao, D. Handler, P. Karpowicz, et al. 2011. A genome-scale shRNA resource for transgenic RNAi in Drosophila. *Nat. Methods.* 8:405–407. http://dx.doi.org/10.1038/nmeth.1592

Sarov, M., C. Barz, H. Jambor, M.Y. Hein, C. Schmied, D. Suchold, B. Stender, S. Janosch, V.V. K J, R.T. Krishnan, et al. 2016. A genome-wide resource for the analysis of protein localisation in Drosophila. *eLife.* 5:e12068. http://dx.doi.org/10.7554/eLife.12068

Schindelin, J., I. Arganda-Carreras, E. Frise, V. Kaynig, M. Longair, T. Pietzsch, S. Preibisch, C. Rueden, S. Saalfeld, B. Schmid, et al. 2012. Fiji: an open-source platform for biological-image analysis. *Nat. Methods.* 9:676–682. http://dx.doi.org/10.1038/nmeth.2019

Somers, W.G., and R. Saint. 2003. A RhoGEF and Rho family GTPase-activating protein complex links the contractile ring to cortical microtubules at the onset of cytokinesis. *Dev. Cell.* 4:29–39. http://dx.doi.org/10.1016/S1534-5807(02)00402-1

Sonnemann, K.J., and W.M. Bement. 2011. Wound repair: toward understanding and integration of single-cell and multicellular wound responses. *Annu. Rev. Cell Dev. Biol.* 27:237–263. http://dx.doi.org/10.1146/annurev-cellbio-092910-154251

Spradling, A.C. 1986. P element-mediated transformation. *In* Drosophila: A practical approach. D.B. Roberts, editor. IRL Press, Oxford. 175–197.

Team, R.C. 2016. R: A language and environment for statistical computing. *In* R Foundation for Statistical Computing, Vienna, Austria. Available at https://www.R-project.org/ (accessed December 10, 2016).

Terasaki, M., K. Miyake, and P.L. McNeil. 1997. Large plasma membrane disruptions are rapidly resealed by Ca^{2+}-dependent vesicle-vesicle fusion events. *J. Cell Biol.* 139:63–74. http://dx.doi.org/10.1083/jcb.139.1.63

Urbanek, S. 2013. tiff: Read and write TIFF images. *In* R package version 0.1-5. Available at https://CRAN.R-project.org/package=tiff (accessed December 10, 2016).

Vaughan, E.M., A.L. Miller, H.-Y.E. Yu, and W.M. Bement. 2011. Control of local Rho GTPase crosstalk by Abr. *Curr. Biol.* 21:270–277. http://dx.doi.org/10.1016/j.cub.2011.01.014

Verboon, J.M., and S.M. Parkhurst. 2015. Rho family GTPases bring a familiar ring to cell wound repair. *Small GTPases.* 6:1–7. http://dx.doi.org/10.4161/21541248.2014.992262

Wenzl, C., S. Yan, P. Laupsien, and J. Grosshans. 2010. Localization of RhoGEF2 during Drosophila cellularization is developmentally controlled by Slam. *Mech. Dev.* 127:371–384. http://dx.doi.org/10.1016/j.mod.2010.01.001

Wickham, H. 2009. ggplot2: Elegant Graphics for Data Analysis. Springer-Verlag, New York. 213 pp.